Multi-level Monte Carlo finite volume methods for nonlinear systems of conservation laws in multi-dimensions

S. Mishra, Ch. Schwab and J. Šukys

MULTI-LEVEL MONTE CARLO FINITE VOLUME METHODS FOR NONLINEAR SYSTEMS OF CONSERVATION LAWS IN MULTI-DIMENSIONS

S. MISHRA, CH. SCHWAB, AND J. ŠUKYS

ABSTRACT. We extend the Multi-Level Monte Carlo (MLMC) algorithm of [19] in order to quantify uncertainty in the solutions of multi-dimensional hyperbolic systems of conservation laws with uncertain initial data. The algorithm is presented and several issues arising in the massively parallel numerical implementation are addressed. In particular, we present a novel load balancing procedure that ensures scalability of the MLMC algorithm on massively parallel hardware. A new code `ALSVID-UQ` is described and applied to simulate uncertain solutions of the Euler equations and ideal MHD equations. Numerical experiments showing the robustness, efficiency and scalability of the proposed algorithm are presented.

1. INTRODUCTION

A number of problems in physics and engineering are modeled in terms of systems of conservation laws:

$$
(1.1) \qquad \begin{aligned}
\mathbf{U}_t + \operatorname{div}(\mathbf{F}(\mathbf{U})) &= 0, \quad \forall (x,t) \in \mathbb{R}^d \times \mathbb{R}_+, \\
\mathbf{U}(x,0) &= \mathbf{U}_0(x),
\end{aligned}
$$

Here, $\mathbf{U} : \mathbf{D} \subset \mathbb{R}^d \mapsto \mathbb{R}^m$ denotes the vector of conserved variables and $\mathbf{F} : \mathbb{R}^m \times \mathbb{R}^m \mapsto \mathbb{R}^{m \times d}$ is the collection of directional flux vectors. The partial differential equation is augmented with initial data $\mathbf{U}_0$.

Examples for conservation laws include the shallow water equations of oceanography, the Euler equations of gas dynamics, the Magnetohydrodynamics (MHD) equations of plasma physics and the equations of non-linear elasticity.

It is well known that solutions of (1.1) in general develop discontinuities or shock waves in finite time even for smooth initial data. Hence, solutions of (1.1) are sought in the sense of distributions, see [6]. Furthermore, additional admissibility criteria or *entropy conditions* are imposed to ensure uniqueness.

As the equations are non-linear, analytical solution formulas are only available in very special situations. Consequently, numerical schemes are the main tools for the study of systems of conservation laws. Many efficient numerical schemes for approximating systems of conservation laws are currently available. They include the

Finite Volume, conservative Finite Difference and Discontinuous Galerkin methods, see [15, 9].

Existing numerical methods for approximating (1.1) require the initial data $\mathbf{U}_0$ as the input. However, in most practical situations, it is not possible to measure this input precisely. The measurement of other inputs like sources, boundary data and coefficients is also prone to uncertainty. This uncertainty in the inputs for (1.1) results in the propagation of uncertainty in the solution. The modeling and approximation of the propagation of uncertainty in the solution due to uncertainty in inputs constitutes the theme of uncertainty quantification (UQ).

Uncertainty in inputs and solutions of PDEs is frequently modeled in a probabilistic manner. The inputs are random fields with prescribed probability laws. The solution is also realized as a random field and the statistical moments of the solutions like the expectation and variance are the quantities of interest.

It is highly non-trivial to develop efficient algorithms for quantifying uncertainty in conservation laws. The biggest challenge lies in the fact that the discontinuities in physical space may lead to the propagation of discontinuities in the probability space. A robust numerical method should be able to deal with these discontinuities. Another challenge lies in dealing with the fact that the number of random sources driving the uncertainty may be very large (possibly infinite).

The design of efficient numerical schemes for quantifying uncertainty in solutions of conservation laws has seen a lot of activity in recent years. The most popular methods are the stochastic Galerkin methods based on generalized Polynomial Chaos (gPC for short). An incomplete list of references on gPC methods for uncertainty quantification in hyperbolic conservation laws includes [2, 5, 16, 26, 21, 27] and other references therein. Although these *deterministic* methods show some promise, they suffer from the disadvantage that they are highly *intrusive*. Existing codes for computing deterministic solutions of conservation laws need to be completely reconfigured for implementation of the gPC based stochastic Galerkin methods. Furthermore, some of the intrusive schemes appear rather difficult to parallelize.

Another class of methods for computational uncertainty quantification in numerical solutions of PDEs are statistical sampling methods, most notably Monte Carlo (MC) sampling. In a MC method, the probability space is *sampled* and the underlying deterministic PDE is solved for each sample. The MC samples of numerical solutions of the PDE are combined into statistical estimates of expectation and other statistical moments of the random solution which are necessary to quantify uncertainty. In uncertainy quantification for hyperbolic scalar conservation laws (SCLs) with random initial data, MC type methods together with Finite Volume (FV) spatio-temporal discretizations of the PDE were proposed in a recent paper [19]. The MCFVM methods were analyzed in the context of a SCL with random initial data and corresponding estimates of the combined discretization and statistical sampling errors were obtained. MC methods are non-intrusive and therefore are very easy to code. Existing deterministic PDE solvers are reused in MC codes. As it was shown in [19], MC methods converge at rate $1/2$ as the number M of MC samples increases. The asymptotic convergence rate $M^{-1/2}$ is non-improvable by the central limit theorem. Therefore, MC methods require a large number of "samples" (with each "sample" involving the numerical solution of (1.1) with a given draw of initial data $\mathbf{U}_0$) in order to ensure low statistical errors. This slow

convergence entails high computational costs for MC type methods. In particular, quantifying uncertainty with MC methods for systems of conservation laws in several space dimensions with moderately high number of sources of uncertainty becomes very costly.

In order to address this drawback of the MC methods, we proposed a novel *Multi-level Monte Carlo* (MLMC) algorithm for SCLs in [19]. Multi-Level MC methods were introduced by S. Heinrich for numerical quadrature [11] and developed by M. Giles to enhance the efficiency of path simulations for Itô stochastic ordinary differential equations in [7, 8]. More recently, MLMC finite element methods for elliptic problems with stochastic coefficients were introduced by Barth, Schwab and Zollinger in [3].

In [19], we presented and analyzed MLMCFVM for SCLs with *random initial data*. Based on our asymptotic error analysis, we derived in [19] an optimized combination of sampling sizes on different levels of spatial and temporal resolution to achieve maximum accuracy in the statistical estimates of first and higher order moments of the random solution. We proved that for first order FV solvers of the SCL, the MLMCFVM obtained in this way allows the computation of approximate statistical moments with the *same accuracy versus cost ratio as a single deterministic solve on the same mesh*. While offering dramatically improved efficiency over standard MC methods, the MLMC FV methods developed in [19] are still totally non-intrusive and are as easy to code and parallelize as traditional, single level MC FV methods. Numerical examples in one space dimension showed that MLMCFVM was orders of magnitude faster than standard MCFVM.

Our main aim in this paper is to extend the MLMCFVM algorithm to systems of conservation laws in several space dimensions. As compared to [19], in the present paper several interesting implementation issues are addressed: due to the massive computational effort entailed by the accurate numerical solution of multi dimensional systems of conservation laws, numerical solves of (1.1) for single samples of random initial data $\mathbf{U}_0$ can not be performed on a single processor. Therefore, in the present paper the MLMC FV algorithm is extended towards several forms of parallelism: parallel computation of large numbers of samples on a coarse grid, and parallelism by mesh partitioning of the (few) samples on the finest grid. To this end, we describe a novel (static) load balancing paradigm for a *scalable* version of the MLMCFVM on a certain class of massively parallel hardware. Although the theoretical MLMC FV convergence results of [19] no longer hold for hyperbolic systems (there are no convergence results for numerical schemes even for systems with deterministic data), the MLMC FV algorithm developed in [19] is tested on a series of hyperbolic benchmark problems and is shown to be robust: the basic conclusions drawn based on the numerical analysis of MLMC FVM for SCL in [19] appear to be applicable also to algorithm design for a wide range of hyperbolic conservation laws. In particular, we consider the Euler equations of gas dynamics and the system of compressible, ideal MHD equations in two space dimensions and show that the MLMCFVM methods can quantify uncertainty in very complex realistic situations; for instance, the MLMC FVM is able to handle a large number of sources of uncertainty (reminiscent to large number of stochastic dimensions in a gPC method) that appear to be beyond the reach of other existing UQ methods for systems of hyperbolic conservation laws.

The rest of the paper is organized as follows: The mathematical setup is described in Section 2. We note that conservation laws with uncertain sources and boundary data can be handled similarly. We present the MC and MLMC algorithms from [19] in Sections 4 and 5, respectively. The serial implementation of the FV solver is briefly recapitulated in Section 6. In Section 7, we describe the parallelization algorithm and numerical experiments in several space dimensions are presented in Section 8.

2. Mathematical Preliminaries

Let $(\Omega, \mathcal{F}, \mathbb{P})$ denote a complete probability space, then:

Definition 2.1 (Random field). *A random field is a measurable mapping* $\mathbf{U} : \Omega \ni \omega \mapsto \mathbf{U}(\mathbf{x}, t, \omega)$ *from* $(\Omega, \mathcal{F})$ *to* $((C([0, \ T], L^1(\mathbb{R}^d)))^m, \ \mathcal{B}((C([0, \ T], L^1(\mathbb{R}^d)))^m)$.

The conservation law (1.1) with random initial data is

$$(2.1) \qquad \begin{aligned} \frac{\partial \mathbf{U}(\mathbf{x}, t, \omega)}{\partial t} + \operatorname{div}(\mathbf{F}(\mathbf{U}(\mathbf{x}, t, \omega))) &= 0, \qquad \mathbf{x} \in \mathbb{R}^d, \quad t > 0, \quad \forall \omega \in \Omega. \\ \mathbf{U}(\mathbf{x}, 0, \omega) &= \mathbf{U}_0(\mathbf{x}, \omega). \end{aligned}$$

Here, the initial data $\mathbf{U}_0$ is a random field i.e, $\mathbf{U}_0 : \Omega \ni \omega \mapsto \mathbf{U}_0(\mathbf{x}, \omega)$ that is a measurable from $(\Omega, \mathcal{F})$ to $((L^1(\mathbb{R}^d))^m, \mathcal{B}((L^1(\mathbb{R}^d))^m))$.

Assuming that the underlying deterministic conservation law (1.1) has an entropy formulation [6, 9], we define the following notion of solutions of (2.1):

Definition 2.2 (Random entropy solution). *A random field* $\mathbf{U} : \Omega \ni \omega \mapsto \mathbf{U}(\mathbf{x}, t, \omega)$ *is an entropy solution to stochastic conservation law* (2.1) *if it is a weak solution and if it satisfies an entropy condition (corresponding to the entropy formulation for* (1.1)*) for* $\mathbb{P}$*-a.e.* $\omega \in \Omega$.

In MLMC methods random entropy solutions are sought path-wise. It is not possible to prove that the random entropy solutions defined above exist for systems of conservation laws. This is not surprising as there are no global well-posedness results for systems of conservation laws, even in one space dimension.

In [19], the authors analyzed the special case of scalar conservation laws with uncertain initial data,

$$(2.2) \qquad \begin{aligned} \frac{\partial u(\mathbf{x}, t, \omega)}{\partial t} + \operatorname{div}(f(u(\mathbf{x}, t, \omega))) &= 0, \qquad \mathbf{x} \in \mathbb{R}^d, \quad t > 0, \quad \forall \omega \in \Omega, \\ u(\mathbf{x}, 0, \omega) &= u_0(\mathbf{x}, \omega). \end{aligned}$$

and showed that the random entropy solutions exist and satisfy certain stability estimates, see Theorem 3.3 of [19]. Furthermore, under suitable regularity assumptions on the initial data, the authors showed that statistical moments of the random entropy solution also exist and are bounded, see Theorem 3.4 of [19].

For the remainder of this paper, we will assume that unique random entropy solutions for the system (2.1) exist. Furthermore, we assume that for $L^1(\mathbb{R}^d)$-valued random initial data with finite variances, this entropy solution has have finite second moments as $L^1(\mathbb{R}^d)^m$-valued random field. Based on this, we generalize the design principles for MLMC FVM from [19] to hyperbolic systems (2.1).

3. Finite volume methods

We aim to design an efficient MC type scheme for approximating the stochastic conservation law (2.1). This entails discretizing space, time as well as the probability space. For spatio-temporal discretization, we will employ finite volume methods.

Let the time step be $\Delta t > 0$ and a triangulation $\mathcal{T}$ of the spatial domain $\mathbf{D} \subset \mathbb{R}^d$ of interest. Here, a triangulation $\mathcal{T}$ will be understood as a partition of the physical domain into a finite set of disjoint open, convex polyhedra $K \subset \mathbb{R}^d$ with boundary being a finite union of plane faces. Let $\Delta x_K := \operatorname{diam} K$ and by $\Delta x(\mathcal{T}) := \max\{\Delta x_K : K \in \mathcal{T}\}$ denote the *mesh width* of $\mathcal{T}$. For any volume $K \in \mathcal{T}$, we define the *set $\mathcal{N}(K)$ of neighboring volumes*

$$(3.1) \qquad \mathcal{N}(K) := \{K' \in \mathcal{T} : K' \neq K \wedge \operatorname{meas}_{d-1}(\overline{K} \cap \overline{K'}) > 0\}.$$

For every $K \in \mathcal{T}$ and $K' \in \mathcal{N}(K)$ denote $\nu_{K,K'}$ to be the unit normal pointing outward from the volume K at the face $\overline{K} \cap \overline{K'}$. We set:

$$(3.2) \qquad \lambda = \Delta t / \min\{\Delta x_K : K \in \mathcal{T}\}$$

by assuming a uniform discretization in time with time step Δt. The constant λ is determined by a standard CFL condition (see [9]) based on the maximum wave speed.

Then, an explicit first-order finite volume ([9]) for approximating (1.1) is given by

$$(3.3) \qquad \mathbf{U}_K^{n+1} = \mathbf{U}_K^n - \frac{\Delta t}{\operatorname{meas}(K)} \sum_{K' \in \mathcal{N}(K)} \mathbf{F}(\mathbf{U}_K^n, \mathbf{U}_{K'}^n),$$

where

$$\mathbf{U}_K^n \approx \frac{1}{\operatorname{meas}(K)} \int_K \mathbf{U}(\mathbf{x}, t^n) d\mathbf{x}$$

is an approximation to the cell average of the solution and $\mathbf{F}(\cdot, \cdot)$ is a numerical flux that is consistent with $\mathbf{F} \cdot \nu_{K,K'}$. Numerical fluxes are usually derived by (approximately) solving Riemann problems at each cell edge resulting in the Godunov, Roe and HLL fluxes, see [15].

Higher order spatial accuracy is obtained by reconstructing $\mathbf{U}$ from $\mathbf{U}_K^n$ in non-oscillatory piecewise polynomial functions or by the Discontinuous Galerkin method. Higher order temporal accuracy is achieved by employing strong stability preserving Runge-Kutta methods.

4. Monte Carlo Finite Volume Method

4.1. **MCFVM algorithm.** The MCFVM algorithm consists of the following three steps:

1. **Sample:** We draw M independent identically distributed (i.i.d.) initial data samples $\mathbf{U}_0^i$ with $i = 1, 2, \cdots, M$ from the random field $\mathbf{U}_0$ and approximate these by piecewise constant cell averages on the FV mesh.
2. **Solve:** For each realization $\mathbf{U}_0^i$, the underlying conservation law (1.1) is solved numerically by the finite volume method (3.3). We denote the finite volume solutions by $\mathbf{U}_K^{i,n}$ for the volume K at time level t^n.

3. Compute **Statistics:** We estimate the expectation of the random solution field with the sample mean (ensemble average) of the approximate solution:

$$(4.1) \qquad E_M[\mathbf{U}_{\mathcal{T}}^n] := \frac{1}{M} \sum_{i=1}^{M} \mathbf{U}_{\mathcal{T}}^{i,n}.$$

Here,

$$\mathbf{U}_{\mathcal{T}}^{i,n}(\mathbf{x}) = \mathbf{U}_K^{i,n}, \quad \forall \quad \mathbf{x} \in K.$$

Higher statistical moments can be approximated analogously.

The above algorithm is quite simple to implement. We remark that step 1 requires a (pseudo) random number generator. In step 2, any standard (high-order) finite volume scheme can be used. Hence, existing code for FVM can be used and there is no need to rewrite FVM code. Furthermore, the only (data) interaction between different samples is in step 3 when ensemble averages are computed. Thus, the MCFVM is non-intrusive as well as easily parallelizable.

4.2. **Convergence analysis.** It is not possible to show rigorously that the MCFVM algorithm converges for systems of conservation laws. In the special case of the stochastic scalar conservation law (2.2), a rigorous error estimate for the MCFVM scheme was obtained in [19]. We refer the reader to [19], Theorem 4.6 for details on the assumptions and directly state the error estimate:

$$(4.2) \qquad \begin{aligned} &\|\mathbb{E}[u(\cdot, t)] - E_M[u_{\mathcal{T}}^n]\|_{L^2(\Omega; L^1(\mathbb{R}^d))} \leq \\ &C \big\{ M^{-\frac{1}{2}} \|u_0\|_{L^2(\Omega; L^1(\mathbb{R}^d))} + t^n \Delta x^s \|TV(u_0(\cdot, \omega))\|_{L^\infty(\Omega; d\mathbb{P})} \big\} \end{aligned}$$

Here, C is a constant independent of M and Δx and s is the convergence rate of the deterministic FVM solver. The results of Kusznetsov [10] show that $s = \frac{1}{2}$, when a first-order FVM is used to approximate scalar conservation laws.

Note that the error estimate for the mean requires that the initial random field has finite second moments. A similar error estimate for the k-th moment was obtained in [19] provided that the initial data has finite $2k$ moments.

Using standard error estimates for numerical schemes approximating scalar conservation laws (see e.g. [9, 19]), it is straightforward to deduce that the (computational) work needed to solve *one* MC sample is, asymptotically,

$$(4.3) \qquad \text{Work}_1(\Delta x) = \mathcal{O}(\Delta x^{-(d+1)})$$

In order to equilibrate the statistical error in (4.2) with the spatio-temporal discretization error, we need to choose

$$(4.4) \qquad M = \mathcal{O}(\Delta x^{-2s})$$

samples. Hence, the amount of computational work needed to solve M samples is

$$(4.5) \qquad \text{Work}_M(\Delta x) = \mathcal{O}(M \Delta x^{-(d+1)}) = \mathcal{O}(\Delta x^{-2s} \Delta x^{-(d+1)}).$$

This leads to the asymptotic error vs. work estimate

$$(4.6) \qquad \|\mathbb{E}[u(\cdot, t^n)] - E_M[u_{\mathcal{T}}^n]\|_{L^2(\Omega; L^1(\mathbb{R}^d))} \lesssim (\text{Work})^{\frac{-s}{(d+1+2s)}}.$$

The above error vs. work estimate should be compared to the deterministic FVM error which scales as $(\text{Work})^{\frac{-s}{(d+1)}}$.

Hence, the MCFVM is considerably more expensive than the standard FVM for a deterministic conservation law. As an example, a first order scheme ($s = 1/2$) leads

to a convergence rate of 1/6 for the MCFVM as compared to a convergence rate of 1/4 for the standard FVM for a deterministic conservation law. Moreover, even for smooth solutions and high order FV schemes, i.e. as $s \to \infty$, the convergence rate is dominated by the MC rate of 1/2.

Remark 4.1. *We are unable to prove a version of the error estimate* (4.2) *for systems of conservation laws. This is primarily on account of the fact that there are no convergence results for numerical schemes approximating* (1.1). *However, we will choose the number of MC samples by* (4.4) *and test numerically whether the above convergence rates and error vs. work estimates hold also for particular hyperbolic systems.*

5. Multi-level Monte Carlo Finite Volume Method

Given the slow convergence of MCFVM, we propose the multi-level Monte Carlo finite volume method (MLMCFVM). The key idea behind MLMCFVM is to simultaneously draw MC samples on a hierarchy of nested grids [19].

5.1. **MLMCFVM algorithm.** The algorithm consists of the following four steps:

1. **Nested meshes:** Consider *nested* triangulations $\{\mathcal{T}_\ell\}_{\ell=0}^\infty$ of the spatial domain $\mathbf{D}$ with corresponding mesh widths Δx_ℓ that satisfy:

$$(5.1) \qquad \Delta x_\ell = \Delta x(\mathcal{T}_\ell) = \sup\{\text{diam}(K): \ K \in \mathcal{T}_\ell\} = O(2^{-\ell}\Delta x_0), \ \ \ell \in \mathbb{N}_0,$$

   where Δx_0 is the mesh width for the coarsest resolution and corresponds to the lowest level $\ell = 0$.

2. **Sample:** For each level of resolution $\ell \in \mathbb{N}_0$, we draw M_ℓ independent identically distributed (i.i.d) samples $\mathbf{U}_{0,\ell}^i$ with $i = 1, 2, \cdots, M_\ell$ from the initial random field $\mathbf{U}_0$.

3. **Solve:** For each resolution level ℓ and each realization $\mathbf{U}_{0,\ell}^i$, the underlying conservation law (1.1) is solved by the finite volume method (3.3) with mesh width Δx_ℓ. Let the finite volume solutions be denoted by $\mathbf{U}_{K,\ell}^{i,n}$ for the volume K and at the time level t^n and resolution level ℓ.

4. **Estimate Solution Statistics:** Fix some positive integer $L < \infty$ corresponding to the highest level. We estimate the expectation of the random solution field with the following estimator:

$$(5.2) \qquad E^L[\mathbf{U}(\cdot, t^n)] := \sum_{\ell=0}^{L} E_{M_l}[\mathbf{U}_{\mathcal{T},\ell}^n - \mathbf{U}_{\mathcal{T},\ell-1}^n],$$

   with E_{M_l} being the MC estimator defined in (4.1) for the level ℓ. Higher statistical moments can be approximated analogously (see, e.g., [19]).

A few remarks are in order. First, the estimator (5.2) indicates that *for each draw of the random data, the hyperbolic system must be solved numerically on two consecutive meshes and time steps, for this data sample.* In the present implementation, we did not exploit this fact to accelerate the solves, e.g. by the use of multilevel techniques, but rather invoked two instances of the deterministic solver `ALSVID` with the same initial data, but different discretization levels.

Second, MLMCFVM is also non-intrusive as any standard FVM code can be used in step 2. Furthermore, MLMCFVM is amenable to efficient parallelization as data from different grid resolutions and different samples only interacts in step 4 where the sample statistics are computed.

5.2. **Convergence analysis.** Again we have rigorous convergence results for the MLMCFVM algorithm in the scalar case (2.2), see Theorem 4.8 of [19] for the assumptions on the grid, the finite volume scheme and the initial data. The resulting error estimate is

$$
\|\mathbb{E}[u(\cdot,t)] - E^L[u(\cdot,t)]\|_{L^2(\Omega;L^1(\mathbb{R}^d))} \leq
$$

(5.3)
$$
\leq C\big\{\bar{t}\,\Delta x_L^s\|TV(u_0)\|_{L^1(\Omega,d\mathbb{P})} + \Delta x_L^s\|u_0\|_{L^\infty(\Omega;W^{s,1}(\mathbb{R}^d))}\big\}
$$
$$
+ C\Big\{\sum_{\ell=0}^{L} M_\ell^{-\frac{1}{2}}\Delta x_\ell^s\Big\}\big\{\|u_0\|_{L^2(\Omega;W^{s,1}(\mathbb{R}^d))} + t\|TV(u_0)\|_{L^2(\Omega;d\mathbb{P})}\big\}\,.
$$

Here s refers to the convergence rate of the deterministic finite volume scheme. From the error estimate (5.3), we obtain that the number of samples to equilibrate the statistical and spatio-temporal discretization errors in (5.2) is given by:

$$
(5.4) \qquad\qquad M_\ell = \mathcal{O}(2^{2(L-\ell)s})
$$

Notice that (5.4) implies that the largest number of MC samples is required on the coarsest mesh level $\ell = 0$, whereas only a small fixed number of MC samples are needed on the finest discretization levels.

Combining (5.2) with (5.4) we obtain the following computational cost (Work$_L$) estimates for the MLMCFVM,

$$
\text{Work}_L = \sum_{\ell=0}^{L} M_\ell \mathcal{O}(\Delta x_\ell^{-(d+1)}) \leq C\sum_{\ell=0}^{L} 2^{2(L-\ell)s+\ell(d+1)} = C2^{2Ls}\sum_{\ell=0}^{L} 2^{(d+1-2s)\ell}
$$

(5.5)
$$
= \begin{cases} C2^{2Ls+[(d+1)-2s]L} = C2^{(d+1)L} = \mathcal{O}(\Delta x_L^{-(d+1)}) & \text{if } s < (d+1)/2, \\ C2^{(d+1)L}(L+1) = \mathcal{O}(\Delta x_L^{-(d+1)}\log_2(\Delta x_L^{-1})) & \text{if } s = (d+1)/2. \end{cases}
$$

Note that the above result is a generalization of the work estimates for MLMCFVM obtained in [19] as we can cover the case of $s = (d+1)/2$.

From the above work estimate, we obtain the corresponding error vs. work estimate for MLMCFVM,
(5.6)

$$
\|\mathbb{E}[u(\cdot,t)] - E_M[u(\cdot,t)]\|_{L^2(\Omega;L^1(\mathbb{R}^d))} \lesssim \begin{cases} (\text{Work})^{-s/(d+1)} & \text{if } s < (d+1)/2, \\ \left(\frac{\text{Work}}{\log(\text{Work})}\right)^{-s/(d+1)} & \text{if } s = (d+1)/2. \end{cases}
$$

The above estimates show that the MLMCFVM is superior to the MCFVM since the asymptotic computational cost for MLMCFVM scales as $\text{Work}^{\frac{-s}{d+1}}$; compare to $\text{Work}^{\frac{-s}{d+1+2s}}$ for the MCFVM scheme. Furthermore, if $s < (d+1)/2$ then this error vs. work estimate is exactly of the same order as the error vs. work of the deterministic finite volume scheme. Hence, the MLMCFVM is expected to be considerably faster than the MCFVM for the same magnitude of error.

Remark 5.1. *Although we are unable to prove rigorously an error estimate like (5.3) for systems of conservation laws, we choose the number of samples at each resolution level by (5.4) and test numerically whether the MLMCFVM for systems obeys the same asymptotic estimates. This is done in the next section.*

6. Serial Implementation of MLMCFVM

We begin the description of implementation of the MLMCFVM algorithm by presenting its implementation on a single processor. The implementation on a parallel architecture is more intricate and is postponed to the next section.

As stated in the last section, the MLMCFVM algorithm has four stages. We discuss implementation issues that arise in each stage below.

6.1. **Step 1: Hierarchy of nested grids.** We will solve systems of conservation laws (2.1) in one and two space dimensions. In two space dimensions, we choose Cartesian meshes for simplicity. It is relatively straightforward to choose a hierarchy of nested grids in both one and two space dimensions.

6.2. **Step 2: Sample.** In this step, we have to draw M_ℓ i.i.d. samples for the initial random field $\mathbf{U}_0$ corresponding to the underlying probability distribution. Standard random number generators (RNG) can be readily used to draw such samples. For the serial implementation, any reasonable RNG works well in practice.

6.3. **Step 3: Solve.** For each realization of the initial random field, we need to solve (2.1) with a finite volume scheme. In this paper, we consider two numerical examples. First, the Euler equations of gas dynamics are considered. In several space dimensions, these equations are

$$\rho_t + \operatorname{div}(\rho \mathbf{u}) = 0,$$
$$(6.1) \qquad (\rho \mathbf{u})_t + \operatorname{div}(\rho \mathbf{u} \otimes \mathbf{u} + p\mathbf{ID}) = 0,$$
$$E_t + \operatorname{div}((E + p)\mathbf{u}) = 0.$$

Here, ρ is the density and $\mathbf{u}$ is the velocity field. The pressure p and total energy E are related by the ideal gas equation of state:

$$(6.2) \qquad E := \frac{p}{\gamma - 1} + \frac{1}{2}\rho|\mathbf{u}|^2,$$

with γ being the ratio of specific heats. It is well known that the Euler equations are strictly hyperbolic and the corresponding eigenvalues and eigenvectors are readily computed, see [15].

The second numerical example that we will consider are the equations of Magnetohydrodynamics (MHD) given by

$$\rho_t + \operatorname{div}(\rho \mathbf{u}) = 0,$$
$$(\rho \mathbf{u})_t + \operatorname{div}(\rho \mathbf{u} \otimes \mathbf{u} + (p + \frac{1}{2}|\mathbf{B}|^2)I - \mathbf{B} \otimes \mathbf{B}) = 0,$$
$$(6.3) \qquad \mathbf{B}_t + \operatorname{div}(\mathbf{u} \otimes \mathbf{B} - \mathbf{B} \otimes \mathbf{u}) = 0,$$
$$E_t + \operatorname{div}((E + p + \frac{1}{2}|\mathbf{B}|^2)\mathbf{u} - (\mathbf{u} \cdot \mathbf{B})\mathbf{B}) = 0,$$
$$\operatorname{div}(\mathbf{B}) = 0,$$

Here, $\mathbf{B}$ denotes the magnetic field and the total energy is given by the equation of state:

$$(6.4) \qquad E := \frac{p}{\gamma - 1} + \frac{1}{2}\rho|\mathbf{u}|^2 + \frac{1}{2}|\mathbf{B}|^2.$$

In contrast to the Euler equations, the MHD equations are not strictly hyperbolic. Furthermore, the design of robust numerical schemes for MHD is quite challenging

as the equations (6.3) involve the divergence constraint. This constraint needs to be handled in a suitable manner in order to avoid spurious oscillations, see [25]. Note that the Euler equations (6.1) are recovered from the MHD equations (6.3) by setting the magnetic field $\mathbf{B} \equiv 0$.

As the solve step in the MLMCFVM algorithm will be repeated for a large number of samples on different space-time resolution levels, we need a robust and efficient FVM code for the Euler and MHD equations. We choose the code named `ALSVID` [1] that was designed by researchers at CMA, University of Oslo and SAM, ETH Zürich. As `ALSVID` is extensively used in the examples of this paper, we describe it briefly below.

6.3.1. *ALSVID.* This finite volume code approximates the Euler equations and MHD equations in one, two and three space dimensions. It is based on the following ingredients:

1. **Approximate Riemann solver:** The numerical fluxes in the finite volume scheme (3.3) used in `ALSVID` are based on approximate Riemann solvers of the HLL type. For the Euler equations (6.1), the code uses the HLL three wave solver proposed by Toro et. al [24]. This approximate Riemann solver resolves contact discontinuities and has the same resolution as the standard Roe solver but computationally is less expensive and is known to preserve positive densities and pressures in the absence of round-off errors, see [13].

   For the MHD equations (6.3), `ALSVID` uses the three and five wave HLL type solvers designed in [13]. These solvers aim at approximating the modified Godunov-Powell form of the MHD equations, see [22, 13].

2. **Divergence constraint.** The divergence constraint in the MHD equations (6.3) is handled in `ALSVID` by adding the Godunov-Powell source term to the MHD equations. This source term is proportional to the divergence and allows divergence errors to be swept out of the domain. Numerical stability can only be ensured by a careful *upwinding* of the source term, see [13].

3. **Non-oscillatory reconstructions.** `ALSVID` employs a variety of piecewise polynomial non-oscillatory reconstruction procedures for attaining high order of spatial accuracy. In particular, second order ENO and WENO procedures are employed, see section 2 of [13].

   However, these procedures need to be modified in order to preserve positivity of the density and pressure. Such modifications are described in section 2 of [13].

4. **Time stepping.** High-order accurate time stepping procedures of the SSP Runge-Kutta [14] are employed in `ALSVID`.

Fluxes on the boundary of the computational domain are defined using so-called ghost cells, see chapter 10 in [15].

`ALSVID` uses a modular structure in `C++` with a `Python` front end for pre- and post-processing. One and two dimensional visualizations are performed with `MatPlotLib` and three dimensional data sets are visualized using `MayaVi2`. Extensive testing of `ALSVID` has been performed and reported in [13].

6.4. **Computing sample statistics.** For both MCFVM and MLMCFVM algorithms we need to combine individual realizations to compute ensemble averages. It is straightforward to compute the sample mean for the MCFVM and the estimator

(5.2) for MLMCFVM. A straightforward algorithm to compute an *unbiased* estimate of the variance for scalar $u = u(x, t)$ with fixed x, t is the following statistical estimator:

$$(6.5) \quad \text{Var}[u] := \mathbb{E}[u^2] - \mathbb{E}[u]^2 \approx \text{Var}_M[u] := \frac{1}{M-1} \sum_{i=1}^{M} (u^i)^2 - \left(\frac{1}{M-1} \sum_{i=1}^{M} u^i \right)^2$$

where u^i are MCFVM samples. This way, it suffices to loop over all samples only once; unfortunately, both quantities are almost equal in the regions of vanishing variance which leads to *subtractive cancellation* and *loss of accuracy* in floating point arithmetic. In [28], the authors propose an alternative *stable* "on-line" variance computation algorithm:

Set $\bar{u}^0 = 0$ and $\Phi^0 = 0$; then proceed iteratively:

$$(6.6) \qquad \bar{u}^i \quad = \quad \sum_{j=1}^{i} u^j / i$$

$$(6.7) \qquad \Phi^i \quad := \quad \sum_{j=1}^{i} (u^j - \bar{u}^i)^2 = \Phi^{i-1} + (u^i - \bar{u}^i)(u^i - \bar{u}^{i-1})$$

Then, the unbiased mean and variance estimates are given by:

$$(6.8) \qquad\qquad E_M[u] = \bar{u}^M, \quad \text{Var}_M[u] = \Phi^M / (M-1).$$

Although identical in exact arithmetic, the above algorithm can deal with small cancellation errors.

We combine a standard RNG in step 2, `ASLVID` in step 3 and the above estimators in step 4 to obtain an efficient MLMCFVM for a single processor. The resulting code is also written in `C++` with `Python` front and back ends. Note that the deterministic code `ALSVID` is reused without any alterations in the solve step as MCFVM and MLMCFVM are non-intrusive. As the UQ module is based on `ALSVID`, we call it as `ALSVID-UQ`. The parallel version of `ALSVID-UQ` will be described later.

6.5. **Numerical experiments for systems in 1D.** We describe numerical experiments for one dimensional systems of conservation laws to test `ALSVID-UQ`.

6.5.1. *Sod shock tube with uncertain shock location.* Let $Y \sim 1 + \mathcal{U}(0, \frac{1}{10})$ be a random variable. We consider the one dimensional version of the Euler equations (6.1) with *random* initial shock with *uncertain* location (near $x = 1$):

$$(6.9) \quad \mathbf{U}_0(x, \omega) = \{\rho_0(x, \omega), u_0(x, \omega), p_0(x, \omega)\} = \begin{cases} \{3.0, 0.0, 3.0\} & \text{if} \quad x < Y(\omega), \\ \{1.0, 0.0, 1.0\} & \text{if} \quad x > Y(\omega). \end{cases}$$

The initial data (6.9) and the reference MLMC solution at time $t = 0.5$ are depicted in Figure 1. At every point $x \in [0, 2]$ the solid line represents the mean and the dashed lines represent the mean $\pm$ standard deviation of the (random) solution. For each *sample* the initial shock splits into three waves: a left going rarefaction wave, a right going contact discontinuity and a right going shock wave. Notice the improvement of the regularity in the stochastic solution: deterministic path-wise solutions for each sample are discontinuous due to formation of the shock and the contact; nevertheless, the mean of the solution is continuous. In [20], a detailed regularity analysis for these quantities is given, as well as a mathematical analysis

of the space-time regularity of statistical moments, as well as for (generalized) polynomial chaos coefficients.
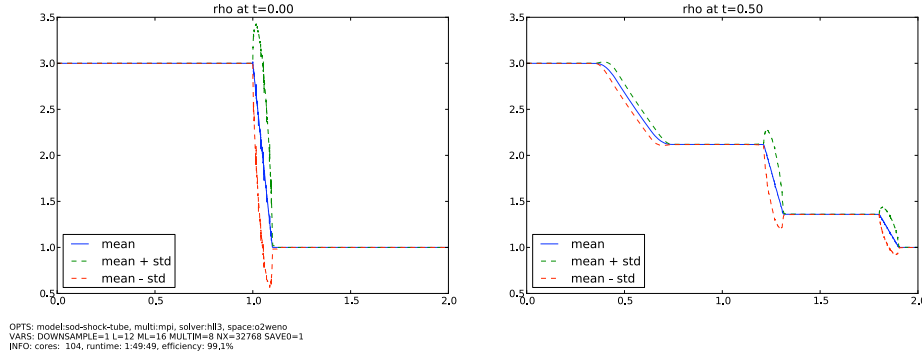
FIGURE 1. Reference solution using MLMCFVM. Initial shock splits into 3 waves all having uncertain location. The resulting ensemble average is *more regular* (continuous) than its paths (with shocks).

Remark 6.1. *The "overshoots" in dashed lines representing standard deviation do* not *imply that the random shock amplitude can exceed the mean depicted in solid line; in fact, the shock amplitude is the same for every sample path.*

Remark 6.2. *The small font lines (OPTS, VARS and INFO) in the lower left corner of every figure indicate the parameters of the simulation. Detailed explanation of these parameters is provided in the tables below;*

OPTS	description
equation	system of conservation laws
model	initial data (always specified explicitly)
multi	parallelization type (single (serial) or mpi)
solver	Godunov-type solver (hll, hll3, hll5, etc.)
space	spacial reconstruction

VARS	description
ML	number of samples at the finest mesh level (M_L)
L	number of hierarchical mesh levels (L)
NX, NY	number of cells in X and in Y directions
MULTIM	#cores for MC samples ($samplers_L$)
MULTIX	#cores in X direction for domain decomposition
MULTIY	#cores in Y direction for domain decomposition

INFO	description
cores	total number of cores used in the simulation
runtime	clock-time (serial runs) or wall-time (parallel runs); hrs:min:sec
efficiency	MPI efficiency, as defined in (7.9)

Remark. Using the notation from subsection 7.2, we infer the identity:

$$subdomains_L = \text{MULTIX} \times \text{MULTIY}.$$

6.5.2. *Numerical convergence analysis.* Using MLMCFVM approximation from Figure 1 as a reference solution, we run MCFVM and MLMCFVM methods on the series of mesh resolutions ranging from 32 cells up to 8192 cells and monitor the convergence behavior. The number of levels for the MLMCFVM method is chosen so that the coarsest level contains 8 cells.

Error estimator. Since the solution is a random field, the discretization error is a random quantity as well. For convergence analysis we therefore compute a statistical estimator by averaging estimated discretization errors from several independent runs. We will compute the error in (4.2) by approximating $L^2(\Omega; L^1(\mathbb{R}^d))$ norm with MC quadrature. Let U_{ref} denote the reference solution and $\{U_k\}_{k=1,\dots,K}$ be a sequence of independent approximate solutions obtained by running MCFVM or MLMCFVM solver K times corresponding to K realizations of the stochastic space. Then the $L^2(\Omega; L^1(\mathbb{R}^d))$-based relative error estimator is defined as in [19],

$$(6.10) \qquad \mathcal{RE} = \sqrt{\sum_{k=1}^{K} (\mathcal{RE}_k)^2 / K}$$

where:

$$(6.11) \qquad \mathcal{RE}_k = 100 \times \frac{\|U_{\text{ref}} - U_k\|_{l^1}}{\|U_{\text{ref}}\|_{l^1}}$$

The extensive analysis for the appropriate choice of K is conducted in [19]; we choose $K = 30$ which was shown to be more than sufficient.

Notation. Notation for different combinations of ML(MC) and FVM methods:

MC	Monte Carlo with 1st order FVM scheme	$M = \mathcal{O}(\Delta x^{-1})$
MC2	Monte Carlo with 2nd order FVM scheme	$M = \mathcal{O}(\Delta x^{-2})$
MLMC	multilevel MC with 1st order FVM scheme	$M_\ell = M_L 2^{(L-\ell)}$
MLMC2	multilevel MC with 2nd order FVM scheme	$M_\ell = M_L 4^{(L-\ell)}$

The parameter M_L corresponds to the number of samples in the finest level and can be freely chosen. Analysis in [19] suggests that $M_L = 16$ is a reasonable choice; however, $M_L = 4$ yielded better results for the problems with particularly large number of levels. In the convergence analysis we choose $M_L = 16$ unless indicated otherwise. Having notations and definitions in place, we proceed to the convergence plots of mean and variance.

Dashed lines in Figure 2 (and all subsequent figures) indicate *expected* convergence rate slopes obtained by theory for *scalar* case (see (4.2) and (5.3)). We expect them to coincide with the observed convergence rates for *systems* of conservation laws and in this particular case they are actually very similar. Findings coincide with the results published in [19] confirming the robustness of the implementation.

Remark. Convergence rate for MLMC2 w.r.t. runtime is achieved *only asymptotically* due to additional $\log_2(\text{Work})$ term for the case $s = (d+1)/2$ in (5.6).

In Figure 3, we show convergence plots for variance. The observed convergence rate for MLMC2 is again slightly smaller than expected. This could be attributed to two reasons. First, as indicated before, the optimal convergence rate is only expected asymptotically when $s = (d+1)/2$ which is the case for formally second order schemes in one space dimension. We assume that second order schemes
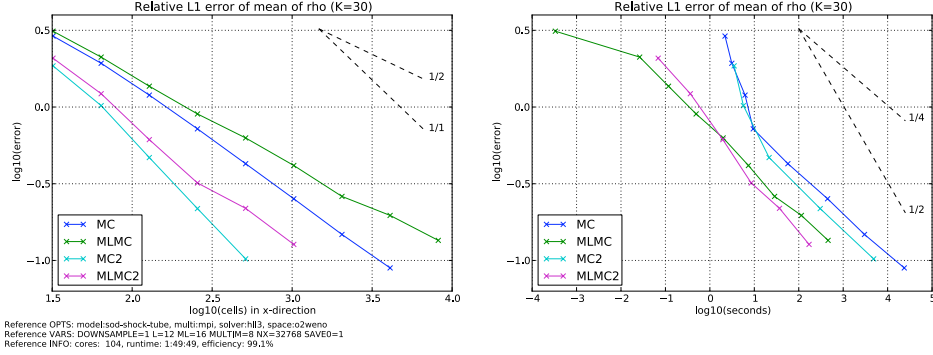
FIGURE 2. Convergence of mean for 1-D Euler. Both MLMC (MLMC2) and MC (MC2) give similar errors for the same spatial resolution. However, there is a significant difference in runtime: multi-level MC methods are almost 2 orders of magnitude faster that pure MC.
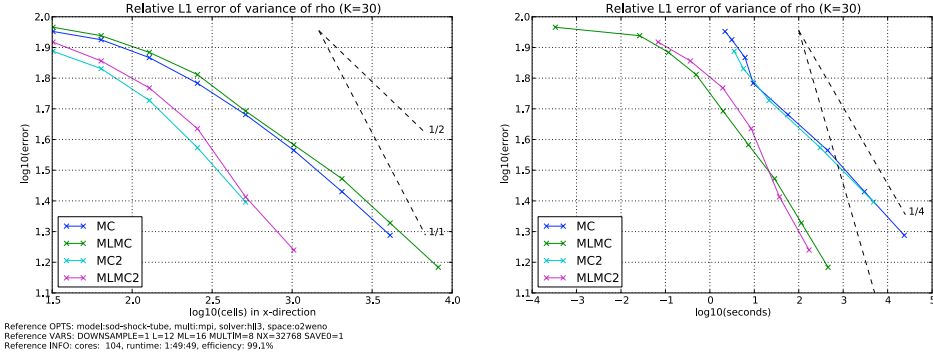
FIGURE 3. Convergence of variance for 1-D Euler.

converge with rate one in the presence of shocks. The second reason could be the amplitude of the fourth moment as the error estimate of the variance relies on the fourth moment. We compute the the 4th centered moment in Figure 4 and find that it is of relatively small amplitude.

The results in the above figures clearly show that the second order methods are more efficient (faster) than the corresponding first order methods. Moreover, the MLMC(2) methods are more than two orders of magnitude faster than the MC(2) methods in computing the mean as well as in computing the variance.

7. PARALLEL IMPLEMENTATION OF MLMCFVM

We recall that MLMC consists of four steps. In the first step, we select a nested hierarchy of triangulations. This step is straightforward for any parallel architecture. In step 2, we draw samples for the initial random field with a given probability distribution. Here, we need a robust random number generator (RNG) described below.
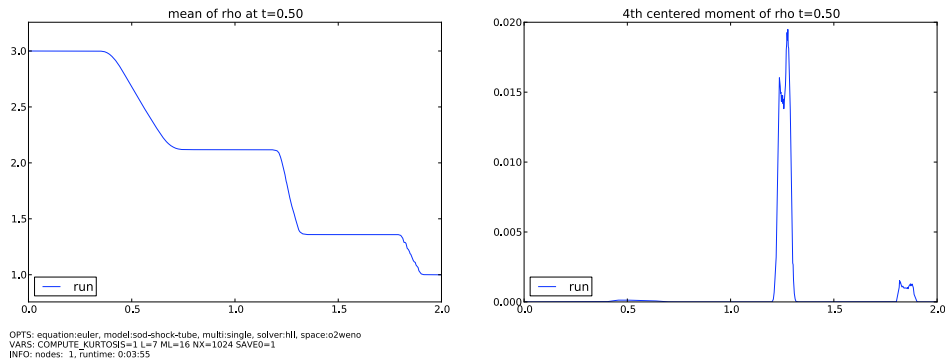
FIGURE 4. 4th centered moment using MLMC

7.1. **Robust pseudo random number generation.** Random number generation becomes a very sensitive part of Monte Carlo type algorithms on massively parallel architectures. Inconsistent seeding and insufficient period length of the RNG might cause correlations in presumably i.i.d. draws which might potentially lead to biased solutions such as in Figure 5.
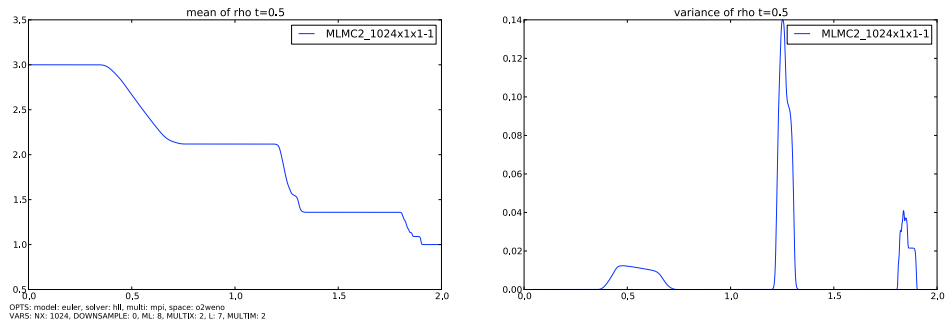
FIGURE 5. A parallel MLMC2 run with faulty seeding and short RNG period - solution becomes biased and variance is no longer symmetric around shocks.

Such spurious correlations are due to two factors: firstly, for a large number of MC samples, we need a longer period and hence a larger buffer of the RNG. Secondly, the seeding of the buffer for each core must be done very carefully to preserve statistical independence.

For the numerical simulations reported below, we used the WELL-series of pseudo random number generators from [18, 17]. These generators have been designed with particular attention towards large periods and good equidistribution. To deal with the seeding issues, we *injectively* (i.e. one-to-one) map the *unique* rank of each core to some corresponding element in the hardcoded array of prime numbers (henceforth, the array of seeds). In this way the independence is preserved. *Different* random solutions needed for error estimates (6.10) in convergence analysis can be obtained by introducing a deterministic shift on the hardcoded array of seeds; this shift must be sufficiently large to guarantee non-overlapping sets of seeds.

For all numerical experiments reported in this paper the RNG `WELL512a` was used. We found `WELL512a` to have a sufficiently large period $2^{512} - 1$ and to be reasonably efficient (33 CPU sec for 10^9 draws). We emphasize that there are plenty of alternatives to `WELL512a` with even longer periods (which, however, use more memory than `WELL512a`). To name a few: `WELL1024a` with period $2^{1024} - 1$, takes 34 sec and `WELLRNG44497` with period $2^{44497} - 1$ which takes 41 sec to generate 10^9 draws.

In step 3 of the MLMCFVM algorithm, we solve the conservation law (2.1) for each draw of the initial data. This is performed with `ALSVID`. A massively parallel version of `ALSVID` has already been developed for deterministic problems; refer to [1] for further details. The parallelization paradigm for `ALSVID` is based on domain decomposition using Message Passing Interface (`MPI`) standard and its particular implementation `OpenMPI`. Refer to [29] and [30] for detailed descriptions of `MPI` and `OpenMPI`, respectively. For the sake of consistency, we briefly recapitulate frequently used terms:

core   an independent unit running the program in parallel with other such units. We assume one `MPI` processes per every core.
node   multiple cores sharing the same physical memory.
sample initial data computed for some particular random draw of ω.

The key issue in the parallel implementation of the solve step is to distribute computational work evenly among the cores. In what follows, we assume *a homogenous computing environment* meaning that all cores are assumed to have identical CPUs and RAM per node, and equal bandwidth and latency to all other cores. Next, we describe our load balancing strategy.

7.2. **Static load balancing.** There are 3 levels of parallelization: over mesh resolution levels, over MC samples and *inside* the deterministic solver using domain decomposition. Domain decomposition parallelization is used only in the few levels with the finest mesh resolution. On these levels, the number of MC samples is small. However, these levels require most of the computational effort (unless $s = (d+1)/2$ in (5.5) holds). For the finest mesh level $\ell = L$ we *fix* the number of cores:

$$(7.1) \qquad \underbrace{cores_L}_{\text{\# of cores}} = \underbrace{subdomains_L}_{\text{\# of subdomains}} \times \underbrace{samplers_L}_{\text{\# of groups for MC samples}}$$

Then, the number of cores for all the remaining levels $(cores_{L-1}, \ldots, cores_0)$ are computed using the *a-priori* work estimates from (4.3) combined with (5.4):

$$(7.2) \qquad \frac{\text{Work}_{M_\ell}(\Delta x_\ell)}{\text{Work}_{M_{l-1}}(\Delta x_{\ell-1})} \sim \frac{M_L 2^{2(L-\ell)s}\Delta x_\ell^{-(d+1)}}{M_L 2^{2(L-(\ell-1))s}\Delta x_{\ell-1}^{-(d+1)}} = \frac{2^{-2\ell s}}{2^{-2(\ell+1)s}2^{-(d+1)}} = 2^{d+1-2s}$$

In this way the positive integer parameters $subdomains_L$ and $samplers_L \leq M_L$ recursively determine the number of cores needed for each level $\ell < L$:

$$(7.3) \qquad cores_\ell = \left\lceil \frac{cores_{\ell+1}}{2^{d+1-2s}} \right\rceil, \quad \forall \ell < L.$$

Notice, that the denominator 2^{d+1-2s} in (7.3) is a *positive integer* (a power of 2) provided $s \in \mathbb{N}/2$ and $s \leq (d+1)/2$ (the latter is *not* an additional constraint as it is also present in (5.6)). However, when $s < (d+1)/2$, we have:

$$(7.4) \qquad 2^{d+1-2s} \geq 2$$

which (when L is large) leads to inefficient load distribution for levels $\ell \leq \ell^*$, where:

$$(7.5) \qquad \ell^* := \min\{0 \leq \ell \leq L : cores_{\ell+1} < 2^{d+1-2s}\}$$

We investigate the amount of *total* work required for "inefficient" levels $\ell \in \{0, \ldots, \ell^*\}$:

$$(7.6) \qquad \begin{aligned} \text{Work}_{\{0,\ldots,\ell^*\}} :&= \sum_{\ell=0}^{\ell^*} \text{Work}_\ell \overset{(7.2)}{=} \sum_{\ell=0}^{\ell^*} \frac{\text{Work}_{\ell^*}}{2^{(d+1-2s)(\ell^*-\ell)}} \leq \sum_{\ell=-\infty}^{\ell^*} \frac{\text{Work}_{\ell^*}}{2^{(d+1-2s)(\ell^*-\ell)}} \\ &= \frac{\text{Work}_{\ell^*}}{1-(2^{d+1-2s})^{-1}} \overset{(7.4)}{\leq} \frac{\text{Work}_{\ell^*}}{1-\frac{1}{2}} = 2 \cdot \text{Work}_{\ell^*} \end{aligned}$$

For the sake of simplicity, assume that $samplers_L$ and $subdomains_L$ are nonnegative integer powers of 2. Under this assumption, definition (7.5) of ℓ^* together with recurrence relation (7.3) *without* rounding up ($\lceil \cdot \rceil$) implies that $cores_{\ell^*} \leq 1/2$. Hence, total work estimate (7.6) for *all* levels $\ell \in \{0, \ldots, \ell^*\}$ translates into an estimate for sufficient number of cores, which, instead of $\ell^* + 1$, turns out to be *only* 1:

$$(7.7) \qquad \text{Work}_{\{0,\ldots,\ell^*\}} \leq 2 \cdot \text{Work}_{\ell^*} \quad \longrightarrow \quad cores_{\{0,\ldots,\ell^*\}} \leq 2 \cdot \frac{1}{2} = 1$$

The implementation of (7.7) (i.e. multiple levels per 1 core) is *essential* to obtain highly scalable and efficient parallelization of MLMC-FVM schemes with $s < \frac{d+1}{2}$.

The example of static load distribution for MLMC-FVM algorithm using all three parallelization levels is given in Figure 6, where the parameters are set to:

$$L = 5, \quad M_L = 4, \quad d = 1, \quad s = \frac{1}{2}, \quad subdomains_L = 2, \quad samplers_L = 4.$$
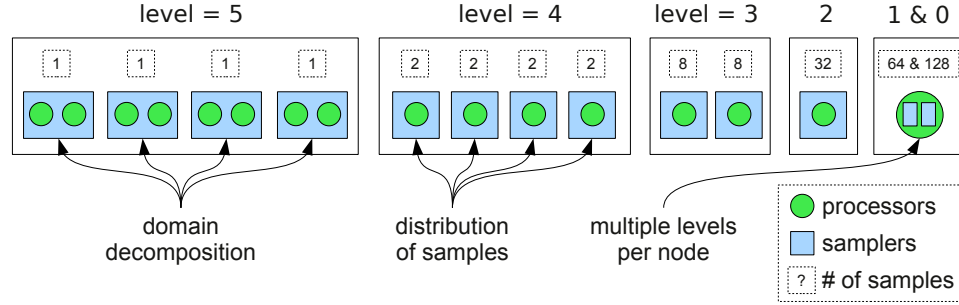
FIGURE 6. Static load distribution structure

This concludes the discussion of static load balancing and of step 3. In step 4 of MLMCFVM, we combine the results to compute sample mean and variance. Special attention needs to be paid to the computation of variance.

7.3. **Variance computation for parallel runs.** Assume we have 2 cores A and B each computing M_A and M_B ($M = M_A + M_B$) number of samples respectively. Then keeping the notation and definitions as in the previous section, the *unbiased*

estimate for mean and variance can be obtained by: (see [4])

$$E_M[u] = \frac{M_A E_{M_A}[u] + M_B E_{M_B}[u]}{M},$$

$$\delta = E_{M_B}[u] - E_{M_A}[u],$$

(7.8)

$$\Phi^M = \Phi^{M_A} + \Phi^{M_B} + \delta^2 \cdot \frac{M_A \cdot M_B}{M},$$

$$\mathrm{Var}_M[u] = \frac{\Phi^M}{M-1}.$$

This algorithm (7.8) is then recursively extended to arbitrary finite number of cores by combining any two of them until only one is left.

7.4. **Parallelization results.** To verify the reliability of the parallelization procedure, we repeat the convergence analysis simulations that were conducted with the serial version of the algorithm in the last section.

The error vs. resolution plot should be identical and the error vs. runtime plot should have longer runtimes due to parallelization overhead. We observe this behavior in Figure 7 and Figure 8. The runtime of the *parallel* algorithm is obtained by measuring the so-called *wall-time*, i.e. the total time passed during the simulation. The wall-time is accessible as `MPI_Wtime()` routine in `MPI2.0`. It is always larger than CPU clock time since additionally it takes into account the time consumed by the operating system, networking, waiting or other auxiliary processes present on the core. In the convergence plots we use *cumulative wall-time* (obtained by adding wall-times from each core); this way the dependence on the used number of cores is reduced allowing for straightforward comparison of the results.
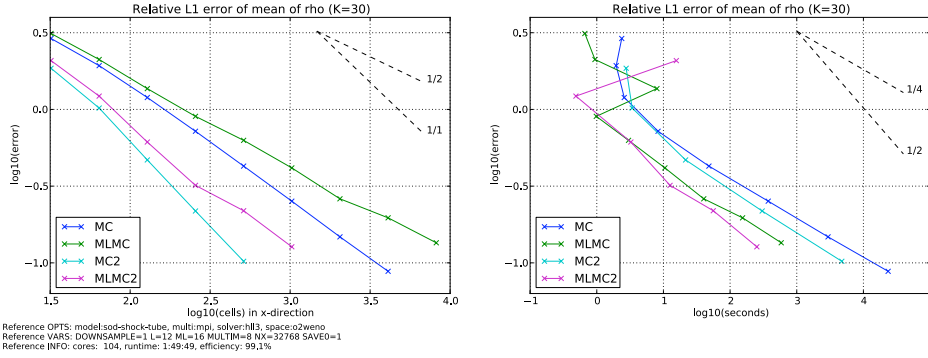
FIGURE 7. Convergence of mean is consistent with convergence of mean for the *serial* version of the algorithm in Figure 2.

7.5. **Efficiency and Scaling.** In Figure 9, we investigate the parallelization efficiency for the convergence analysis conducted in the previous subsection. The parallel efficiency is defined as

(7.9) $\text{efficiency} := \dfrac{(\text{cumulative wall-time}) - (\text{cumulative wall-time of MPI calls})}{\text{cumulative wall-time}}$
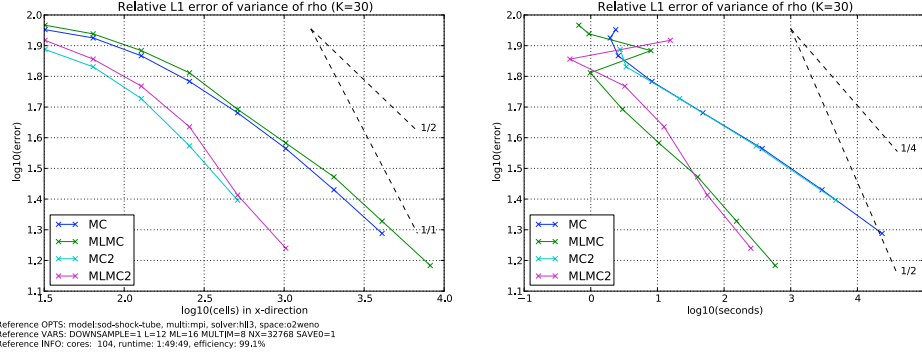
FIGURE 8. Convergence of variance is consistent with convergence of variance for the *serial* version of the algorithm in Figure 3.
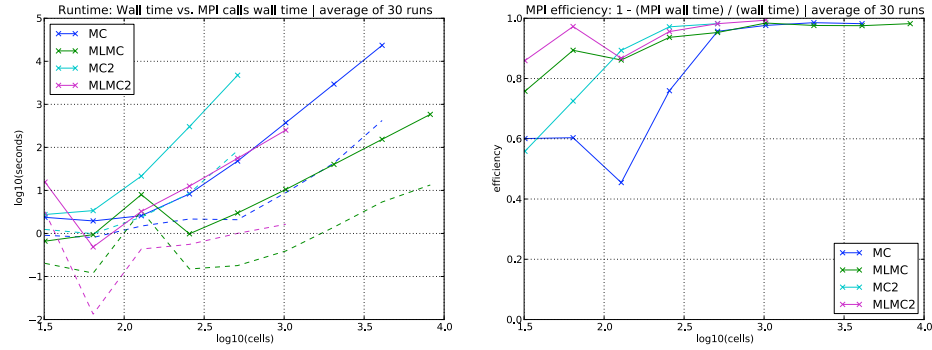
FIGURE 9. MPI efficiency of the convergence analysis simulations in Figure 7 and Figure 8. For large problems (more than 256 cells) the parallelization is very efficient - only negligible amount of runtime is spent on auxiliary networking and waiting.

It separates the amount of time spent in computing from the amount of time spent in communicating (the latter is indicated with *dashed* lines in runtime plots). We see that high efficiency ($\sim 98\%$) is achieved for large problems.

Furthermore, in Figure 10 we verify *strong scaling* (fixed discretization and sampling parameters while increasing #cores) of the parallel algorithm and in Figure 11 we verify *weak scaling* (problem size is equivalent to #cores) of our implementation. We observe that our implementation scales linearly (strongly) upto 200 cores. Similarly, weak scaling is also realized upto 200 cores. We believe that our parallelization algorithm will scale linearly for a much larger number of cores. Numerical investigation of scaling for massively parallel versions of `ALSVID-UQ` will be reported in forthcoming papers.

8. NUMERICAL EXPERIMENTS FOR SYSTEMS IN 2D

The efficient parallelization of `ALSVID` in the previous section provides us with a robust and efficient cod e (`ALSVID-UQ`) for uncertainty quantification in hyperbolic systems of conservation laws. Consequently, we are able to conduct large scale
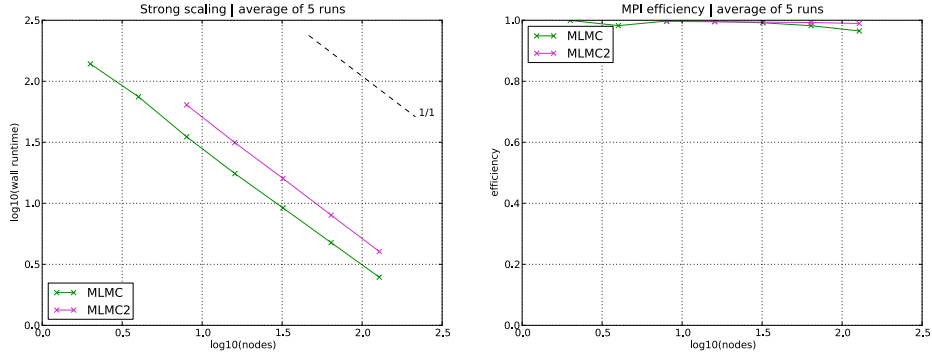
FIGURE 10. Strong scaling. Domain decomposition parallelization is enabled from $10^{1.5}$ cores onwards (for MLMC only); its scalability is inferior to pure (ML)MC parallelization due to additional networking between sub-domain boundaries.
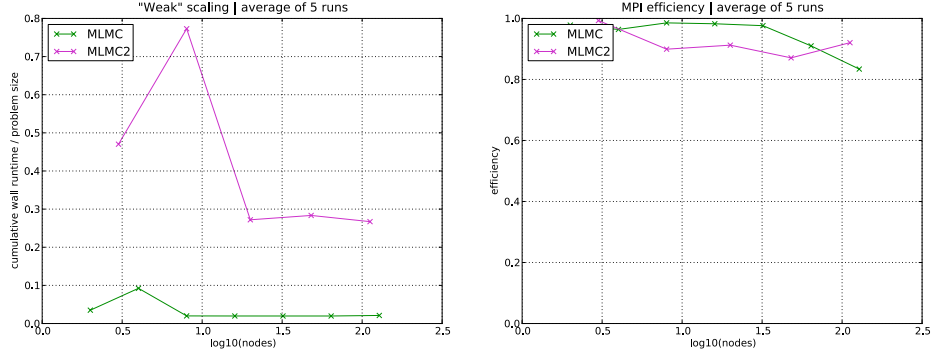
FIGURE 11. Weak scaling. Analogously as in Figure 10, the slight deterioration in MLMC scaling from $10^{1.5}$ cores onwards could have been caused by inferior scaling of domain decomposition method.

numerical experiments in $d = 2$ (and possibly $d = 3$) space dimensions. Note that quantification of uncertainty poses a considerably larger challenge than that of a single run of the deterministic solver since a large number of samples (or stochastic dimensions in gPC based methods) are needed.

8.1. Euler equations of gas dynamics.
We consider Euler equation of gas dynamics (6.1) in two space dimensions. We conduct two numerical experiments for the Euler equations and report the results below.

8.1.1. Shock-vortex interaction.
In this standard test case for deterministic solvers (see [23]), the computational domain is taken to be $[0, 1] \times [0, 1]$. Let $Y \sim \frac{1}{2} + \mathcal{U}(0, \frac{1}{10})$. The initial *random* stationary Mach 1.1 shock is normal to x axis and has

uncertain location with mean at $\mathbf{x}_1 = \frac{1}{2} + \frac{1}{20}$. The resulting initial data are:
(8.1)
$$\{\rho_0(\mathbf{x},\omega),\ \mathbf{u}_0(\mathbf{x},\omega),\ p_0(\mathbf{x},\omega)\} = \begin{cases} \{1,\ (\sqrt{\gamma},\ 0)^\top,\ 1\} & \text{if} \quad \mathbf{x}_1 < Y(\omega), \\ \{\dfrac{1}{1.1},\ (1.1\sqrt{\gamma},\ 0)^\top,\ 1 - \dfrac{\gamma}{10}\} & \text{if} \quad \mathbf{x}_1 > Y(\omega). \end{cases}$$

This base flow is superposed with the a vortex centered at (x_c, y_c):

$$(8.2) \qquad \bar{\mathbf{u}}_0(\mathbf{x},\omega) = (\epsilon\tau e^{\alpha(1-\tau^2)}\sin\theta,\ -\epsilon\tau e^{\alpha(1-\tau^2)}\cos\theta)^\top$$

$$(8.3) \qquad \bar{p}_0(\mathbf{x},\omega) = -(\gamma-1)\frac{\epsilon^2 e^{2\alpha(1-\tau^2)}}{4\alpha\gamma\rho}$$

where:
(8.4)
$$r = \sqrt{(\mathbf{x}_1 - x_c)^2 + (\mathbf{x}_2 - y_c)^2}, \quad \tau = \frac{r}{r_c}, \quad \sin\theta = \frac{\mathbf{x}_2 - y_c}{r}, \quad \cos\theta = \frac{\mathbf{x}_1 - x_c}{r}.$$

and we choose the parameters to be:

$$(8.5) \qquad \epsilon = 0.3, \quad r_c = 0.05, \quad \alpha = 0.204, \quad x_c = 0.25, \quad y_c = 0.5.$$

OPTS: equation:euler, model:shockvortex, multi:mpi, solver:hll3, space:o2wenof
VARS: DOWNSAMPLE=1 L=8 ML=16 MULTIM=16 MULTIX=2 MULTIY=2 NX=2048 NY=2048
INFO: cores: 128, runtime: 5:47:15, efficiency: 91.6%
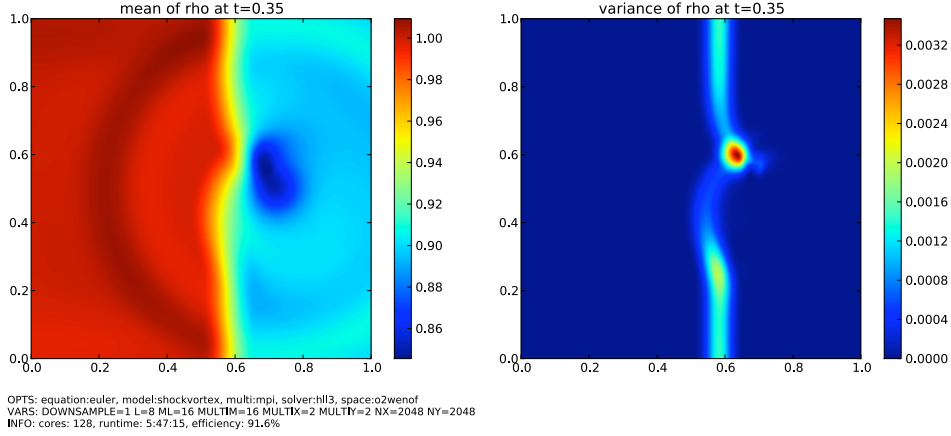
FIGURE 12. Shock-vortex interaction solution at time $t = 0.35$ using MLMC

The location of the initial stationary supersonic shock is uncertain in this experiment. For each realization of the initial data, the pathwise solution consists of the vortex moving to the right, interacting with the shock and emerging out of the shock. Since the shock location is uncertain, we expect the mean to be *smoother* than the pathwise solutions. A priori, it is unclear how the variance is going to be redistributed.

The results of uncertain shock-vortex interaction simulation at time $t = 0.35$ are given in Figure 12. At this time instant, the vortex has just emerged out of the shock. We present results for a MLMC run with a second-order WENO discretization in physical space. The HLLC solver is used for computing the numerical fluxes. The results are computed on 9 nested levels of resolution ($L = 8$) with the finest resolution being on a 2048×2048 mesh and with timesteps reduced accordingly in order to maintain the same CFL constant over all discretization levels.

The simulation is run on 128 cores and 16 samples are taken for the finest mesh resolution.

The results in Figure 12 show that the MLMC-WENO scheme is quite robust. The mean of the pressure shows that the stationary shock (with uncertain location) is smoothed out. Similarly, the vortex (in mean) has emerged from the shock at this time instant. The vortex is resolved quite sharply. The plot for the variance of the pressure is more interesting. Although the initial variance was concentrated on the shock, we see that the variance is redistributed by the flow. A large proportion of the variance is still concentrated on the shock. However, the profile is deviated near the point where the vortex was incident at the shock. Furthermore, there is a clear signature of the vortex in the variance although the vortex (in mean) has already crossed the shock. The above experiment reveals that the variance (and possibly higher moments) can have a much more complex behavior than the mean flow field. It requires a very efficient numerical method to be able to resolve such complex features.

8.1.2. *Cloud shock.* So far, we have presented numerical experiments for the Euler equations with only one source of uncertainty - uniformly random initial shock location. In reality, the number of uncertainty sources can be quite large. Stochastic Galerkin methods based on gPC expansions will be deficient at resolving such problems as the computational complexity grows exponentially with the number of uncertainty sources (number of stochastic dimensions or terms in the gPC expansion). On the other hand, methods that are based on MC-sampling scale favourably with respect to high dimension of the parameter space. As an example, consider uncertain initial data with a large number of sources for uncertainty. There is a very negligible increase of computational cost over the case of a single source of uncertainty as a random vector (with the number of components corresponding to the number of uncertainty sources) is drawn instead of a random number at each mesh point and only at the initial time step. If the boundary conditions or sources are uncertain, then the computational cost increases only *linearly* w.r.t. the number of uncertain parameters.

We put the above hypothesis to test on a problem with a high number of uncertainty sources. We consider the so-called *cloud-shock* interaction problem from [12]. The computational domain is taken to be $[0,1] \times [0,1]$. Let $Y \sim \frac{1}{25} + \mathcal{U}(0, \frac{1}{50})$ and let $Y_1, ..., Y_7 \sim \mathcal{U}(0,1)$ be i.i.d. random variables independent from Y.

The initial data consists of an initial shock with the uncertain amplitude and uncertain location and is given by:
(8.6)
$$\{\rho_0(\mathbf{x}, \omega),\ \mathbf{u}_0(\mathbf{x}, \omega),\ p_0(\mathbf{x}, \omega)\} =$$

$$= \begin{cases} \{3.86859 + \dfrac{1}{10} Y_6(\omega),\ (11.2536,\ 0)^\top,\ 167.345 + Y_7(\omega)\} & \text{if} \quad \mathbf{x}_1 < Y(\omega), \\ \{1,\ (0,\ 0)^\top,\ 1\} & \text{if} \quad \mathbf{x}_1 > Y(\omega). \end{cases}$$

Furthermore, a high density cloud or bubble with uncertain amplitude and uncertain shape of the form

(8.7)
$$\rho_{\mathbf{0}}(\mathbf{x}, \omega) = 10 + \frac{1}{2}Y_1(\omega) + Y_2(\omega)\sin(4(\mathbf{x}_1 - 0.25)) + \frac{1}{2}Y_3(\omega)\cos(8(\mathbf{x}_2 - 0.5))$$
$$\text{if} \quad r \leq 0.13 + \frac{1}{50}Y_4(\omega)\sin\theta + \frac{1}{100}Y_5(\omega)\sin(10\theta),$$

where

(8.8)
$$r = \sqrt{(\mathbf{x}_1 - 0.25)^2 + (\mathbf{x}_2 - 0.5)^2}, \quad \theta = \frac{\mathbf{x}_1 - 0.25}{r},$$

lies to the right of the shock. The mean and the variance of the initial data is depicted in Figure 13(a). Note that there are 8 sources of uncertainty in the above problem. A parametric representation of the initial data results in a 11 dimensional problem consisting of two space, one time and eight stochastic dimensions. To the best of our knowledge, such high dimensional problems have not been considered in the literature.

The mean and variance of the solution at time $t = 0.06$ is shown in Figure 13(b). The results are from a MLMC-WENO run with 9 nested levels of resolution ($L = 8$) and the finest resolution is set to 2048×2048 mesh. The number M_L of MC samples at the finest resolution is 8 and number of cores for this run is 128. Note that time taken for this simulation is comparable to that for the shock-vortex interaction where we had only one source of uncertainty. This justifies our claim that MLMC methods are robust with respect to a high number of sources of uncertainty.

The physics of the flow in this case consists of the supersonic initial shock moving to the right, interacting with the high density bubble and leading to a complex flow pattern that consists of a leading bow shock, trailing tail shocks and a very complex region (near the center) possessing sharp gradients as well as turbulent like smooth features. The mean flow (for the density) consists of the bow shock, tail shocks and a complex region with sharp gradients as well as smooth regions. The variance is concentrated in the smooth region at the center; it is significantly smaller at the tail shocks and almost vanishing at the bow shock. The initial uncertainty in the shape of the bubble seems to lead to a more complex distribution of the variance.

8.2. **MHD equations of plasma physics.** Next, we describe a couple of numerical experiments for MHD equations of plasma physics.

8.2.1. *Orszag-Tang vortex.* The deterministic version of the Orszag-Tang vortex is the standard benchmark for MHD codes. We adapt it to include stochastic initial data. The computational domain is taken to be $[0, 2] \times [0, 2]$. Let $Y_1, Y_2 \sim \mathcal{U}(0, 1)$. The standard initial data (from [25]) for the Orszag-Tang vortex is *randomly* perturbed: the phases of the velocities are uncertain and depend on the scaled random variables Y_1 and Y_2:

(8.9)
$$\{\rho_0(\mathbf{x}, \omega), \ \mathbf{u}_0(\mathbf{x}, \omega)\} = \{\gamma^2, \ (-\sin(\pi\mathbf{x}_2 + \frac{1}{20}Y_1(\omega)), \ \sin(\pi\mathbf{x}_1 + \frac{1}{10}Y_2(\omega)))^\top\},$$
$$\{p_0(\mathbf{x}, \omega), \ \mathbf{B}(\mathbf{x}, \omega)\} = \{\gamma, \ (-\sin(\pi\mathbf{x}_2), \ \sin(2\pi\mathbf{x}_1))^\top\}.$$

The mean field and the variance (for the plasma density) are shown in Figure 14. The computation is performed using the MLMCFVM scheme with second-order WENO reconstruction, and with the HLL three wave solver of [13]. The code uses

OPTS: equation:euler, model:cloudshock-euler, multi:mpi, solver:hll3, space:o2wenof
VARS: CFL=0.4 DOWNSAMPLE=1 L=8 ML=8 MULTIM=4 MULTIX=4 MULTIY=4 NX=2048 NY=2048 SAVE0=1
INFO: cores: 128, runtime: 6:06:44, efficiency: 92.2%

(a) initial data

OPTS: equation:euler, model:cloudshock-euler, multi:mpi, solver:hll3, space:o2wenof
VARS: CFL=0.4 DOWNSAMPLE=1 L=8 ML=8 MULTIM=4 MULTIX=4 MULTIY=4 NX=2048 NY=2048 SAVE0=1
INFO: cores: 128, runtime: 6:06:44, efficiency: 92.2%

(b) solution at $t = 0.06$

FIGURE 13. Cloud shock at $t = 0$ and $t = 0.06$ using MLMC-FVM

an upwind discretization of the Godunov-Powell source term. The results shown in this figure are from a computation with 8 levels of refinement ($L = 7$) and the finest mesh resolution of 2048×2048 mesh points. The number of MC samples at the finest resolution is 4. The problem has more than 10^9 degrees of freedom per time step and the total number of time steps is about 10^4 making the computational volume of problem between 10^{12} and 10^{13}. These numbers show that the simulation is extremely challenging and requires massively parallel architectures. In fact, the above problem took about 6 hours (wall-clock) on 128 cores.

It is well known (see [25, 13]) that stable computation of numerical solutions of the Orszag-Tang problem on very fine meshes is quite challenging. Since our spatial resolution at mesh level $L = 7$ is very fine, we need an *extremely* robust code like ALSVID for the solve step in MLMCFVM in order to resolve this problem.

OPTS: model:orszagtang, multi:mpi, solver:hll3, space:o2wenof
VARS: DOWNSAMPLE=1 L=7 ML=4 MULTIM=1 MULTIX=8 MULTIY=8 NX=2048 NY=2048
INFO: cores: 128, runtime: 5:22:33, efficiency: 89.3%
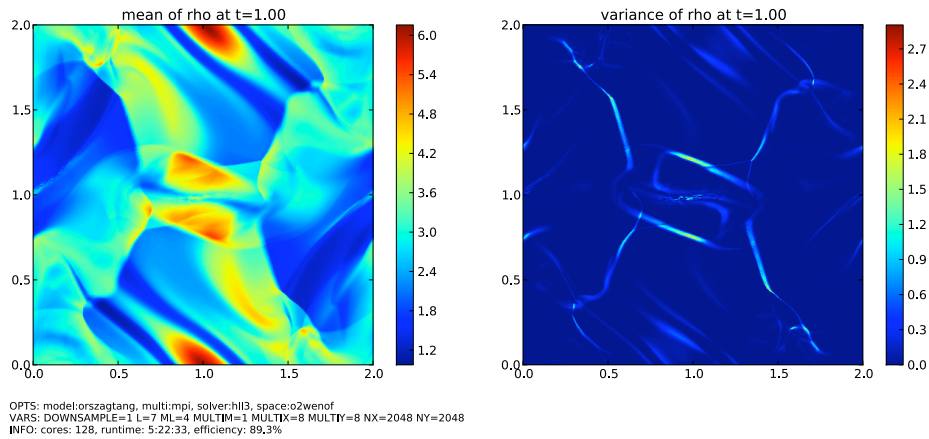
FIGURE 14. Uncertain Orszag-Tang vortex solution at $t = 1.0$ using MLMC-FVM. Variance is very large near discontinuities of the path-wise solutions.

The mean density is quite complicated with shocks along the diagonals of the domain as well a (smooth) current sheet at the center of the domain. The solution consists of discontinuities interspersed within interesting smooth features. Our simulations show that the variance is concentrated at shocks as well as at the current sheets and other interesting smooth regions. From this problem as well as the results of the previous section, we observe that the variance is a very good indicator of where the discontinuities and sharp gradients of the solution are concentrated and would serve a good *a posteriori* error indicator for adaptive mesh refinement.

8.2.2. *Numerical convergence analysis.* We analyze this particular two dimensional numerical experiment in greater detail. We investigate convergence of error vs. work in Figure 15 and Figure 16. The error in the mean field converges at expected rates. At comparable numerical resolution and accuracy, the MLMC(2) is about two orders of magnitude faster than the MC(2) method for this problem. We observe a slight deterioration in the estimated convergence rates for the variance. This could well be a pre-asymptotic effect. As seen in Figure 16, the curves are steeping which seems to indicate better rates with further refinement. Again, the MLMC(2) appears considerably faster than the corresponding MC(2) method in delivering variance estimates of comparable numerical accuracy.

8.2.3. *Efficiency of parallelization.* We test the efficiency of static load balancing for parallelization procedure described in section 7 in this two-dimensional example. In Figure 17, we show the parallelization efficiency of the MLMCFVM and see that the algorithm is quite efficient and most of the time is spent computing rather than communicating or waiting.

The strong scaling for this problem is shown in Figure 18. We see that the algorithm scales linearly to around 200 cores. Similarly, Figure 19 shows a weak scaling upto similar number of processors. We have not tested the algorithm for a larger number of processors but expect it to scale upto a much larger number of
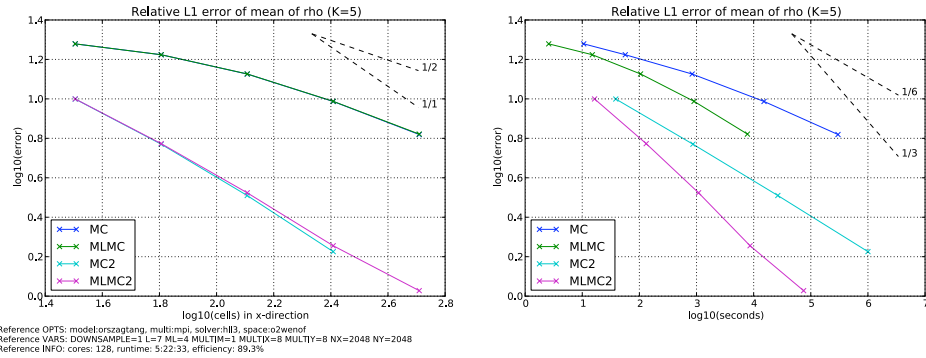
FIGURE 15. Convergence of mean in the uncertain Orszag-Tang vortex simulation.
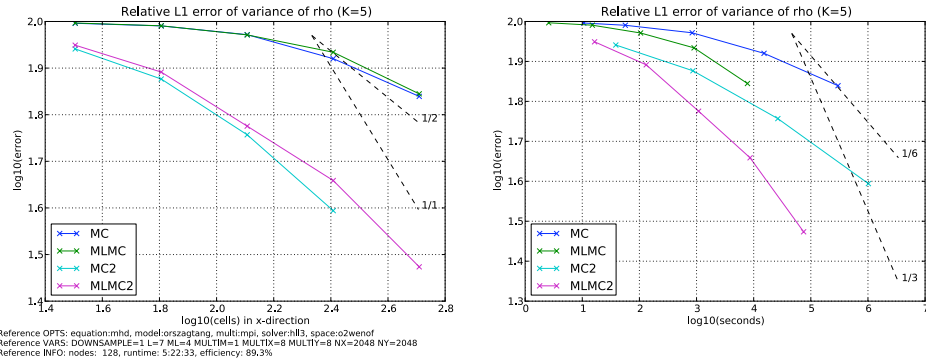
FIGURE 16. Convergence of variance in the uncertain Orszag-Tang vortex simulation.

cores. The results in both one and two space dimensions show that our static load balancing algorithm is quite efficient.
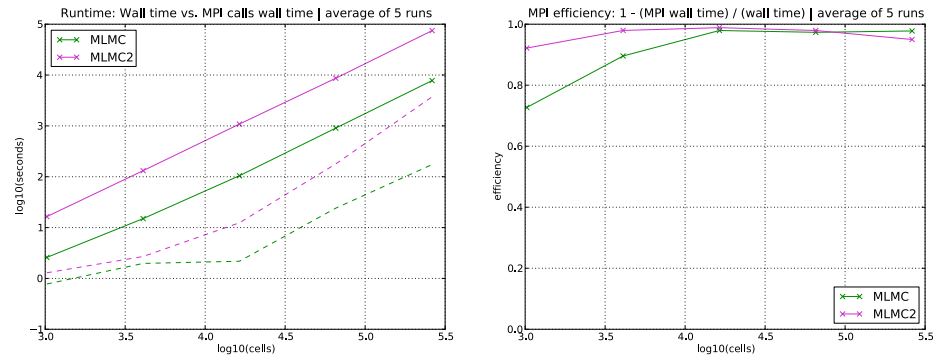
FIGURE 17. MPI overhead. For large problems (more than 64 cells in each dimension) efficiency of parallelization is as good as it was for $d = 1$ experiments in Figure 9.
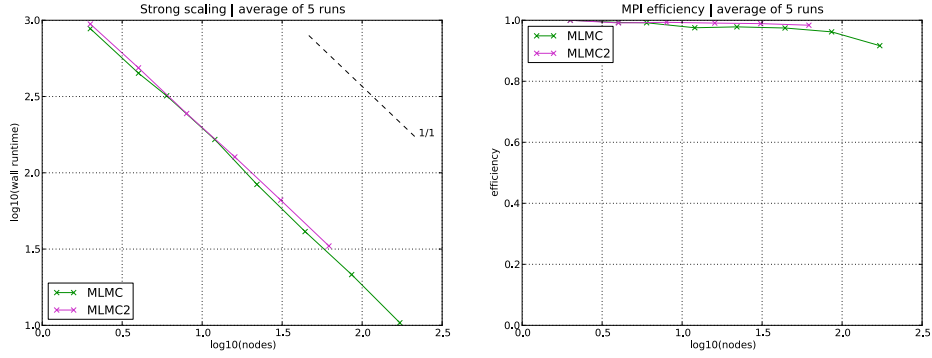
FIGURE 18. Strong scaling.
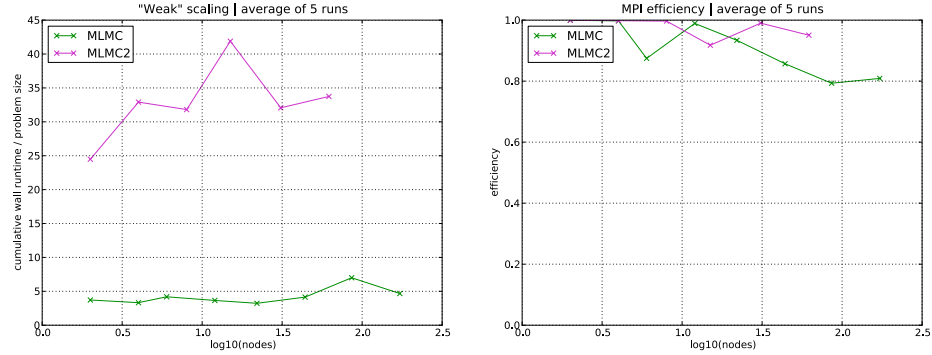
FIGURE 19. Weak scaling.

8.2.4. *Isothermal blast wave.* In the numerical experiments presented so far, we have considered the initial randomness to be uniformly distributed. The MLM-CFVM algorithm allows, however, initial data with any probability distribution which can be sampled numerically. We demonstrate its versatility with respect to the initial probability distribution in the following experiment where the initial uncertainty is distributed normally.

The computational domain for this isothermal blast wave experiment is taken to be $[0, 1] \times [0, 1]$. Let $Y \sim \mathcal{N}(0, 1)$. The magnetic field from the initial data for the deterministic isothermal blast wave is perturbed - its magnitude depends on Y that is drawn from a normal distribution:
(8.10)
$$\rho_0(\mathbf{x}, \omega) = \begin{cases} 100 & \text{if} \quad (\mathbf{x}_1 - \frac{1}{2})^2 + (\mathbf{x}_2 - \frac{1}{2})^2 < (\frac{1}{20})^2, \\ 0 & \text{otherwise.} \end{cases}$$

$$\{\mathbf{u}_0(\mathbf{x}, \omega),\ p_0(\mathbf{x}, \omega),\ \mathbf{B}(\mathbf{x}, \omega)\} = \{(0,\ 0)^\top,\ \rho_0(\mathbf{x}, \omega),\ (\frac{5}{\sqrt{\pi}} + \frac{1}{5}Y(\omega),\ 0)^\top\}.$$

The resulting solution is shown in Figure 20. We present results of a simulation performed with five levels of refinement and with the mesh at the finest level consisting of 256×256 points. The number of samples on the finest level is 4 and the computation is performed on 128 cores.

The results show that the mean plasma density has a rotating profile with the initial blast wave spreading out from the center of the domain. Furthermore, the variance is concentrated at the outer blast wave.

We point out that even a single deterministic run for the isothermal blast wave at mesh level $L = 5$ is known to be challenging, (see, e.g. [13]). Additionally, as the MC and MLMC are based on randomly generated initial scenarios, robustness of the path-wise solver ALSVID is crucial to handle each run. Furthermore, given the time scales of the problem, only a fast method like MLMCFVM can handle such complex problems.

OPTS: equation:mhd, model:isothermal-blast-wave, multi:mpi, solver:hll3, space:o2wenof
VARS: L=5 ML=16 MULTIM=4 MULTIX=4 MULTIY=4 NX=256 NY=256 SAVE0=1
INFO: cores: 126, runtime: 0:37:25, efficiency: 95.2%
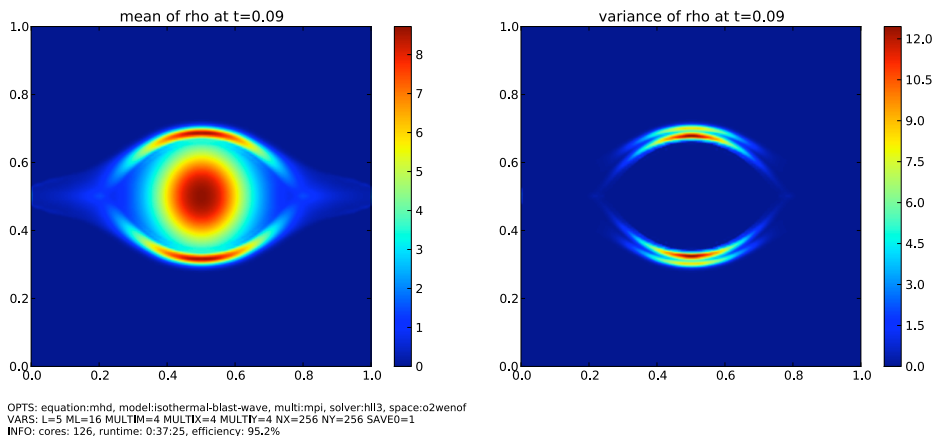
FIGURE 20. Isothermal blast wave solution at $t = 0.09$ using MLMC-FVM with *normally* distributed perturbation of initial magnetic field.

9. Conclusion

We consider systems of conservation laws in several space dimensions but with uncertain initial data. The problem of quantifying the uncertainty in such solutions is quite challenging. In this paper we extend the MLMCFVM of [19] and present it in the context of systems of conservation laws in several space dimensions.

The algorithm is described in detail and some underlying theoretical properties (for scalar conservation laws) are discussed. Several key issues that are encountered in the efficient implementation of this algorithm are presented. They include the choice of the underlying finite volume solver. We choose the ALSVID FVM code [1] as our base code as it provides a robust and efficient approximation of the Euler and MHD equations. Another key issue is the implementation of the MLMC algorithm on parallel architectures. We discuss this issue in considerable detail and propose a novel load balancing procedure of MLMCFVM for parallel architectures.

The MLMCFVM is tested on a suite of one and two dimensional numerical experiments for both Euler as well as MHD equations. We demonstrate that the

MLMCFVM algorithm is robust, efficient and able to resolve very complex flows governed by systems of nonlinear hyperbolic conservation laws with uncertain initial conditions. In particular, this method can handle problems with a large number of stochastic dimensions or sources of uncertainty. Such problems are beyond the reach of other existing methods. Furthermore, the parallel version of `ALSVID-UQ` described here is shown to scale weakly and strongly up to to 200 cores. It is expected to scale substantially beyond this range of cores. We describe several complex flows with random initial data, simulated with MLMCFVM, and emphasize the subtle role played by the non-linearity in the evolution of the variance as well as regularity improvement of the mean due to ensemble averaging.

The main advantages of the MLMCFVM method are its simplicity and non-intrusiveness. It is easy to code and to parallelize. The parallelization can be made more efficient by the load balancing procedure designed in this paper. Furthermore, existing deterministic codes for solving hyperbolic systems of conservation laws can be reused in entirety. Hence, we advocate the use of MLMCFVM algorithms for numerical quantification of uncertainty in solutions of systems of conservation laws. The source code `ALSVID-UQ` can be downloaded from `mlmc.origo.ethz.ch/download`.

We confine ourselves to the case of uncertain initial data in this paper. Uncertain boundary conditions and source terms can be handled analogously. The development of MLMCFVM algorithms for this kind of uncertainty is currently in progress.

References

[1] ALSVID Available from `http://folk.uio.no/mcmurry/amhd`.

[2] R. Abgrall. *A simple, flexible and generic deterministic approach to uncertainty quantification in non-linear problems.* Rapport de Recherche, INRIA, 2007.

[3] A. Barth, Ch. Schwab and N. Zollinger. *Multilevel MC Method for Elliptic PDEs with Stochastic Coefficients.* Report, SAM, 2010 (in review).

[4] T. F. Chan, G. H. Golub. and R. J. LeVeque. *Updating Formulae and a Pairwise Algorithm for Computing Sample Variances.* STAN-CS-79-773, 1979.

[5] Q. Y. Chen, D. Gottlieb and J. S. Hesthaven. *Uncertainty analysis for steady flow in a dual throat nozzle.* J. Comput. Phys, **204**:378-398, 2005.

[6] Constantine M. Dafermos. *Hyperbolic Conservation Laws in Continuum Physics (2nd Ed.).* Springer Verlag (2005).

[7] M. Giles. *Improved multilevel Monte Carlo convergence using the Milstein scheme.* Preprint NA-06/22, Oxford computing lab, Oxford, U.K, 2006.

[8] M. Giles. *Multilevel Monte Carlo path simulation.* Oper. Res., **56**:607-617, 2008.

[9] Edwige Godlewski and Pierre A. Raviart. *Hyperbolic Systems of Conservation Laws.* Mathematiques et Applications, Ellipses Publ., Paris (1991).

[10] Eymard, Robert and Gallouët, Thierry and Herbin, Raphaèle. *Finite volume methods* Handbook of numerical analysis, Vol. **VII**, pp. 713-1020, North-Holland, Amsterdam (2000).

[11] S. Heinrich. *Multilevel Monte Carlo methods.* Large-scale scientific computing, Third international conference LSSC 2001, Sozopol, Bulgaria, 2001, Lecture Notes in Computer Science, Vol **2170**, Springer Verlag (2001), pp. 58-67.

[12] U. S. Fjordholm, S. Mishra and E. Tadmor. *Arbitrarily high-order essentially non-oscillatory entropy stable schemes for systems of conservation laws.* In preparation, 2011.

[13] F. Fuchs, A. D. McMurry, S. Mishra, N. H. Risebro and K. Waagan. *Approximate Riemann solver based high-order finite volume schemes for the Godunov-Powell form of ideal MHD equations in multi-dimensions.* Comm. Comput. Phys., **9**:324-362, 2011.

[14] S. Gottlieb, C. W. Shu and E. Tadmor. *High order time discretizations with strong stability property.* SIAM. Review, **43**:89 - 112, 2001.

[15] R.A. LeVeque. *Numerical Solution of Hyperbolic Conservation Laws.* Cambridge Univ. Press 2005.

[16] G. Lin, C.H. Su and G. E. Karniadakis. *The stochastic piston problem.* PNAS **101**:15840-15845, 2004.

[17] P. L'Ecuyer and F. Panneton. *Fast Random Number Generators Based on Linear Recurrences Modulo 2: Overview and Comparison.* Proceedings of the 2005 Winter Simulation Conference, 110–119, IEEE press, 2005.

[18] P. L'Ecuyer and F. Panneton. *Fast Random Number Generators Based on Linear Recurrences Modulo 2.* ACM Trans. Math. Software, **32**:1-16, 2006.

[19] S. Mishra and Ch. Schwab. *Sparse tensor multi-level Monte Carlo Finite Volume Methods for hyperbolic conservation laws with random initial data.* Preprint 2010, available from `http://www.sam.math.ethz.ch/reports/2010/24`.

[20] S. Mishra, Ch. Schwab and S. Tokareva. *(in preparation)* Working Paper SAM, 2011.

[21] G. Poette, B . Després and D. Lucor. *Uncertainty quantification for systems of conservation laws.* J. Comput. Phys. **228**:2443-2467, 2009.

[22] K. G. Powell, P. L. Roe. T. J. Linde, T . I. Gombosi and D . L. De Zeeuw. *A solution adaptive upwind scheme for ideal MHD.* J. Comp. Phys., **154**(2):284 - 309, 1999.

[23] C. W. Shu. *Essentially non-oscillatory and weighted essentially non-oscillatory schemes for hyperbolic conservation laws.* ICASE Technical report, NASA, 1997.

[24] E. F. Toro, M. Spruce and W. Speares. *Restoration of the contact surface in the Harten-Lax-van Leer Riemann solver.* J. Shock waves, **4**:25-34, 1994.

[25] G. Toth. *The $\mathrm{Div}B = 0$ constraint in shock capturing magnetohydrodynamics codes.* J. Comp. Phys., **161**:605-652, 2000.

[26] J. Tryoen, O. Le Maitre, M. Ndjinga and A. Ern. *Intrusive projection methods with upwinding for uncertain non-linear hyperbolic systems.* Preprint, 2010.

[27] X. Wan and G. E. Karniadakis. *Long-term behaviour of polynomial chaos in stochastic flow simulations.* Comput. Meth. Appl. Mech. Engg. **195**:5582-5596, 2006.

[28] B. P. Welford. *Note on a Method for Calculating Corrected Sums of Squares and Products.* Technometrics, **4**:419-420, 1962.

[29] *MPI: A Message-Passing Interface Standard.* Version 2.2, 2009, available at: `http://www.mpi-forum.org/docs/mpi-2.2/mpi22-report.pdf`.

[30] *Open MPI: Open Source High Performance Computing.* Available at `http://www.open-mpi.org/`.

(Siddhartha Mishra)
Seminar for Applied Mathematics
ETH
HG G. 57.2,
Rämistrasse 101, Zürich, Switzerland.
   E-mail address: `smishra@sam.math.ethz.ch`

(Christoph Schwab)
Seminar for Applied Mathematics
ETH
HG G. 57.1,
Rämistrasse 101, Zürich, Switzerland.
   E-mail address: `christoph.schwab@sam.math.ethz.ch`

(Jonas Šukys)
Seminar for Applied Mathematics
ETH
HG G. 62.1,
Rämistrasse 101, Zürich, Switzerland.
   E-mail address: `jonas.sukys@sam.math.ethz.ch`

Research Reports